PR Internal Mode Extended State Observer-Based Iterative Learning Control for Thrust Ripple Suppression of PMLSM Drives

Guoqiang Zhang, *Senior Member, IEEE*, Xinru Zhao, Qiwei Wang, *Member, IEEE*, Dawei Ding, *Member, IEEE*, Binxing Li, *Member, IEEE*, Gaolin Wang, *Senior Member, IEEE*, and Dianguo Xu, *Fellow, IEEE*

***Abstract*—Permanent magnet linear synchronous motor (PMLSM) suffers from inherent thrust ripples, which cause vibration and noise and worsen the control performance. In this article, an iterative learning thrust ripple suppression method based on a proportional resonant internal model extended state observer (PR-IMESO) is proposed for PMLSM drives. A P-type iterative learning controller (PILC) with the forgetting factor is constructed to suppress the detent force which is the main component of thrust ripples and periodic force ripples. On this basis, PR-IMESO is constructed to further suppress the detent force and the residual disturbance in thrust ripples. In addition, the convergence, stability, and parameter sensitivity of the suppression method are analyzed. The proposed PR-IMESO-based PILC suppression method can suppress thrust ripples of PMLSM pertinently according to their characteristics to achieve overall control performance improvement. Finally, the effectiveness of the proposed method is verified on a 750-W PMLSM experimental platform.**

***Index Terms*—Internal model extended state observer (ESO), iterative learning control (ILC), permanent magnet linear synchronous motor (PMLSM), thrust ripple suppression.**

I. Introduction

PERMANENT magnet linear synchronous motor (PMLSM) can directly generate linear motion without any intermediate transmission device and has the advantages of simple structure, fast dynamic response, high thrust density, etc., which has been widely used in automatic control systems, industrial robots, rail transit, and other occasions [1], [2], [3]. However, because PMLSM has no intermediate transmission device, it is more sensitive to thrust ripples, parameter perturbations, and external disturbances, which worsens the control performance of PMLSM drives [4].

One of the biggest limitations of PMLSM is thrust ripples [5]. The main causes of thrust ripples for PMLSM are the end force, the cogging force, the force ripple, the friction disturbance, the load disturbance, etc. [6]. Due to the breaking of the ends of the core along the moving direction and the primary winding of the motor being discontinuous, PMLSM has a specific periodic thrust ripple, which is called the end force [7]. Same as in the rotating machine, the primary core of PMLSM also uses slotted silicon steel lamination, resulting in the cogging force [7]. Generally, the resultant force of the end force and the cogging force is called the detent force, which is the main reason for thrust ripples of PMLSM. Besides the detent force, periodic force ripples and aperiodic force disturbances are also included in the thrust ripples. The force ripple is mainly caused by current harmonics and back-EMF harmonics [8]. PMLSM is also subjected to viscous friction disturbance and sliding friction disturbance [9]. In addition, since the mover of PMLSM is directly connected to the load, any changes on the load side will be transmitted directly to the motor, resulting in thrust ripples.

Therefore, the thrust ripple components of PMLSM are quite complex, including periodic components, such as the detent force and the force ripple, as well as aperiodic components, such as the friction disturbance and the load disturbance. These not only lead to complex speed harmonic pulsation but also cause vibration and noise, resulting in mechanical damage in severe cases, which has a great impact on the control accuracy of PMLSM drives, especially at low speeds [10].

To further improve the control accuracy and the operation performance of PMLSM drives, it is necessary to effectively suppress the thrust ripples. At present, the research on PMLSM thrust ripple suppression strategy mainly includes two categories: motor design and control algorithm optimization [11]. In terms of improving the motor structure, a modulation method was proposed to reduce the thrust ripples by adjusting the width of the side slots and the lengths of the end teeth [12]. Although this kind of method can essentially improve the negative influence of the motor structure characteristics on mover thrust, it

Manuscript received 8 November 2023; revised 2 April 2024; accepted 27 April 2024. Date of publication 6 May 2024; date of current version 20 June 2024. This work was supported in part by the Research Fund for the National Natural Science Foundation of China under Grant 52177034 and Grant 52125701, in part by Heilongjiang Provincial Natural Science Foundation under Grant YQ2023E016, in part by the Aeronautical Science Foundation of China under Grant ASFC-20220007077002, and in part by the Fundamental Research Funds for the Central Universities under Grant HIT.OCEF.2023003. Recommended for publication by Associate Editor S. Mazumder. *(Corresponding author: Qiwei Wang.)*

The authors are with the School of Electrical Engineering and Automation, Harbin Institute of Technology, Harbin 150001, China (e-mail: zhgq@hit.edu.cn; 22s006090@stu.hit.edu.cn; wqw0543@163.com; dingdawei@hit.edu.cn; lbx@hit.edu.cn; wgl818@hit.edu.cn; xudiang@hit.edu.cn).

Color versions of one or more figures in this article are available at https://doi.org/10.1109/TPEL.2024.3395691.

Digital Object Identifier 10.1109/TPEL.2024.3395691

increases the cost and difficulty of the motor design, and the suppression effect of thrust ripples is limited.

Therefore, many practical and effective control methods were put forward to suppress thrust ripples of PMLSM. These methods fall into two main categories: compensating and suppressing the thrust ripples directly in real time by constructing its model or suppressing it indirectly by reducing the speed fluctuation caused by thrust ripples. The most direct method to suppress thrust ripples is to establish the mathematical model of thrust ripples, and obtain the simplified mathematical model through FEA or online identification, then compensate them in real time. In [13], the method of using FEA data to compensate for the detent force and an observer to compensate for the residual thrust ripples was proposed to reduce thrust ripples of PMLSM. In [14], an online compensation method based on FEA data of the detent force and curve fitting was proposed, and a simple online observer constructed with acceleration was used to observe and compensate the residual thrust ripples. However, these methods all rely on the accurate model of thrust ripples and have a limited suppression effect on thrust ripples of PMLSM.

It is difficult to obtain the model of thrust ripples in the actual system. In view of the periodic characteristic of the detent force for PMLSM, some repetitive and learning control strategies were proposed to suppress thrust ripples, such as periodic adaptive learning control [9], iterative learning control [15], and repetitive control [16]. In [9], a state-periodic adaptive control method was proposed. The key idea is to use one trajectory period past information along the state axis to update the current adaptation law to compensate for the cogging force and the friction force of PMLSM. As a widely used control strategy, iterative learning control (ILC) has a satisfactory suppression effect on periodic disturbances [17]. In [15], a projection-based iterative learning method that utilizes partial but most pertinent information in the error signal was proposed to identify and compensate for the periodic force ripple of PMLSM.

Furthermore, many methods using the observer to indirectly suppress the thrust ripples of PMLSM were proposed, which equates the disturbances of the system to the lumped disturbance to estimate and compensate for it. In [18], a periodic adaptive disturbance observer was proposed to attenuate periodic disturbances in the repetitive motion of PMLSM. However, it is assumed that the disturbances of PMLSM are periodic, and the influence of aperiodic disturbances is not considered. In [19], an augmented generalized proportional-integral observer was presented to estimate and compensate for the disturbance/uncertainty of PMLSM. In [20], a general-purpose two-degree-of-freedom PID type controller integrated with the linear extended state observer (ESO) and the friction feedforward controller was proposed to suppress thrust ripples and nonlinear friction disturbance of PMLSM. However, the traditional ESO can only suppress the disturbances with gradual constants or slow changes and cannot estimate and compensate the periodic disturbances well. In [21], an internal model control with ESO was proposed to reduce the influence of external torque disturbance and moment of inertia variation on the performance of the system, which brings inspiration to PMLSM thrust ripple suppression.

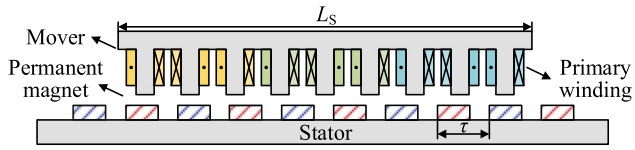

Fig. 1. Schematic diagram of PMLSM.

Aiming at the complex thrust ripple problem of PMLSM, an iterative learning suppression method based on proportional resonant internal model ESO (PR-IMESO) is proposed in this article. First, the thrust ripples of PMLSM are analyzed and modeled. The thrust ripples include the detent force, periodic force ripples, and aperiodic residual thrust ripples, among which the detent force is the main component of thrust ripples and is modeled. A P-type iterative learning controller (PILC) with the forgetting factor is constructed to preliminarily suppress the detent force and periodic force ripples. However, PILC cannot fully eliminate the negative effect of the detent force for PMLSM and has no suppression effect on the aperiodic residual disturbances. On this basis, PR-IMESO considering the detent force model is designed to suppress the residual thrust ripples. The resonant term is introduced into IMESO to strengthen the suppression effect of the fixed-period detent force. The proposed PR-IMESO can suppress the thrust ripples of PMLSM pertinently according to their characteristics to achieve overall control performance improvement. The proposed suppression strategy is almost unaffected by the parameter uncertainty. Finally, the effectiveness of the proposed suppression strategy is verified on a 750-W PMLSM experimental platform.

II. Analysis and Modeling of Thrust Ripples of PMLSM Drives

The structure of PMLSM is shown in Fig. 1, where, L_s is the length of the mover. The thrust is as follows:

$$F_e = \frac{3}{2}\frac{\pi}{\tau} p_n \psi_f i_q \tag{1}$$

where F_e is the electromagnetic thrust, τ is the motor pole distance, p_n is the number of pole pairs, ψ_f is the permanent magnet flux linkage, and i_q is the q-axis current.

The motion equation is expressed as

$$M\frac{dv}{dt} = F_e - F_L + F_d \tag{2}$$

where M is the mover mass, v is the speed of the mover, F_L is the load tension, and F_d is the resultant force disturbance and can be simply described as

$$F_d = F_{det} - B_n v + F_{rip} \tag{3}$$

where F_{det} is the detent force, B_n is the viscous friction coefficient, and F_{rip} refers to other force fluctuations except the detent force and the viscous friction force.

The detent force is the main cause of thrust ripples of PMLSM, which is a periodic function related to the position of the mover [22]. The cogging force and the end force are modeled, respectively, to obtain the detent force model of PMLSM.

When ignoring the end effect, the cogging force of PMLSM can be regarded as the superposition of the interaction force between any primary tooth and all secondary poles. The cogging force of a single tooth can be expressed by Fourier series as

$$f_{\mathrm{cs}} = \sum_{i=1}^{\infty} f_{\mathrm{cs}i} \sin\left(\frac{2\pi i}{\tau}x + \theta_i\right) \tag{4}$$

where $f_{\mathrm{cs}i}$ and θ_i are the amplitude and the phase of the ith harmonic component, respectively, and x is the displacement of the mover.

If the number of teeth for PMLSM is N_{s}, the separation is τ_{s}, and its distribution length corresponds to the number of permanent magnet pole pairs is p, then the resultant cogging force of the whole mover can be expressed as [23]

$$F_{\mathrm{cog}} = \sum_{n=1}^{\infty} f_n N_{\mathrm{s}} \sin\left(\frac{N_{\mathrm{c}} n\pi}{p\tau}x + \varphi_n\right) \tag{5}$$

where N_{c} is the least common multiple of the number of the motor poles $2p$ and the number of the slots N_{s}. From (5), it can be seen that the whole mover cogging force is a function related to the position of the mover, whose period is $2p\tau/N_{\mathrm{c}}$. Therefore, it is also a function with the period of the motor pole pitch τ given as

$$F_{\mathrm{cog}} = \sum_{n=1}^{\infty} a_n \sin\left(\frac{2\pi n}{\tau}x + \alpha_n\right) \tag{6}$$

where a_n and α_n are Fourier series coefficients and phases, respectively.

The end force is a periodic thrust ripple similar to the cogging force. The Fourier series expression of the end force F_{end} is as follows:

$$F_{\mathrm{end}} = \sum_{n=1}^{\infty} b_n \sin\frac{2\pi n}{\tau}\left(x + \frac{\delta}{2}\right) \tag{7}$$

where b_n is the coefficient of the Fourier series, and δ is the phase, expressed as $\delta = m\tau$-L_{s}, where m is an integer.

The resultant force of the end force and the cogging force is called the detent force, which is the main reason for the thrust ripples of PMLSM. According to (6) and (7), the detent force F_{det} can be expressed as

$$F_{\mathrm{det}} = \sum_{n=1}^{\infty} a_n \sin\left(\frac{2\pi n}{\tau}x + \alpha_n\right) + \sum_{n=1}^{\infty} b_n \sin\frac{2\pi n}{\tau}\left(x + \frac{\delta}{2}\right). \tag{8}$$

It can be seen from the mathematical model (8) that the detent force is a function of the mover position with the motor pole pitch τ as the period. The analysis result of the detent force is shown in Fig. 2 [24]. According to the expression of the PMLSM mover speed $v = 2\tau f$, the frequency of the detent force is twice that of the primary winding phase current. The thrust ripple components of PMLSM are numerous and complex, including not only the detent force with large amplitude but also periodic force ripples and aperiodic disturbances with small amplitude, which have a great influence on the operation performance of PMLSM drives.

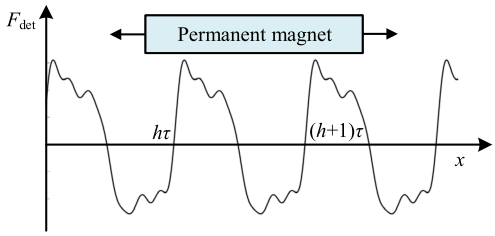

Fig. 2. Analysis result of the detent force.

III. Proposed Thrust Ripple Suppression Strategy With PR-IMESO-Based Iterative Learning Control

A. Scheme of Thrust Ripple Suppression Strategy

The suppression strategy with PR-IMESO-based ILC according to the thrust ripple component characteristics of PMLSM is proposed, as shown in Fig. 3. Because PILC has a good suppression effect on the periodic disturbance without the amplitude, it is used to suppress the detent force, which is the main component of thrust ripples, and the periodic force ripple. On this basis, PR-IMESO considering the detent force model is designed to suppress the residual disturbance. PR-IMESO can suppress not only the modeled detent force but also the other unmodeled complex thrust ripples, including the load disturbance, the current distortion, and the friction force. In addition, the resonant term in the observer is used to strengthen the suppression of the second-order detent force. In this way, the PR-IMESO-based PILC suppression strategy can greatly improve the control performance of PMLSM.

ILC can eliminate the control errors caused by repeated disturbances without an accurate model of the plant. Considering the characteristics of different types of ILC rates and the detent force, this article constructs an open-closed-loop P-type ILC with the forgetting factor to suppress the detent force and periodic force ripples. Combined with the PMLSM drive system, the iterative learning law can be expressed as

$$\begin{cases} u_k(t) = \alpha u_{k-1}(t) + K_{\mathrm{PL1}}\Delta v_{k-1}(t) + K_{\mathrm{PL2}}\Delta v_k(t) \\ \Delta v_k(t) = v_{\mathrm{ref}}(t) - v_k(t) \\ v_k(t) = M(t)\, u_k(t) \end{cases} \tag{9}$$

where α is the forgetting factor. K_{PL1} and K_{PL2} are iterative learning gains. $u_k(t)$, $v_k(t)$, and $\Delta v_k(t)$ are the kth control signal (compensation value of q-axis current), input signal (speed feedback value), and error signal (speed error) of the iterative learning system, respectively. k is the number of iterations. $M(t)$ is the transfer function between the control signal and the output signal of the iterative learning controller. The function of the forgetting factor is to weaken the cumulative effect of aperiodic disturbances and accelerate the convergence speed, whose value is between 0 and 1.

PILC uses the speed error and the compensation value of the q-axis current at the (k-1)th run and the speed error at the kth run to update the current compensation value of the q-axis current to compensate the detent force and force ripples. However, as a conventional method, PILC can only suppress periodic disturbances and has no suppression effect on the aperiodic

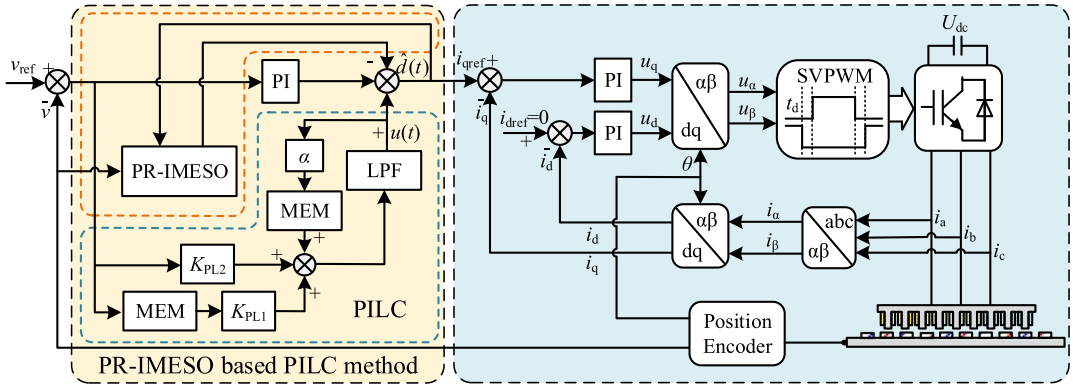

Fig. 3. Proposed PR-IMESO-based PILC thrust ripple suppression method.

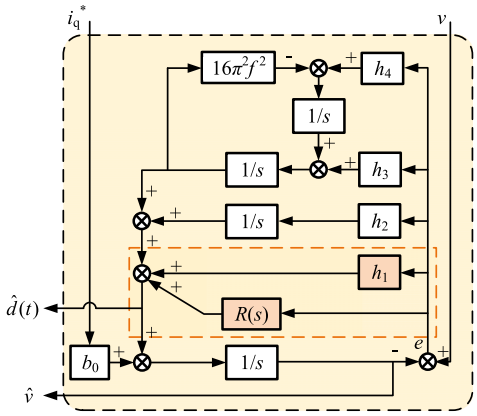

Fig. 4. Block diagram of PR-IMESO.

residual disturbances. Moreover, PILC cannot fully eliminate the negative effect of the detent force for PMLSM. Therefore, PR-IMESO considering the detent force model is designed to suppress the residual disturbance and strengthen the suppression of the detent force. It should be noted that PILC is used to suppress the detent force and the periodic force ripple initially and the resonant term is used to strengthen the suppression effect of the detent force. So PILC and the resonant term in the observer cannot replace each other.

PR-IMESO-based suppression strategy is shown in Fig. 3, which is marked with a yellow dotted box. The input of PR-IMESO is i_{qref} (q-axis current reference) and v (speed feedback value), and the disturbance of PMLSM is estimated by the observer. The output is $\hat{d}(t)$ (a disturbance compensation signal), which is used to correct i_{qref} by feedforward compensation.

The block diagram of PR-IMESO is shown in Fig. 4. As can be seen, IMESO is a fourth-order observer considering the detent force model, and the feedforward proportional term of the error signal and the resonant controller $R(s)$ constitute the proportional resonant controller, then PR-IMESO is obtained.

The quasi-PR controller has a large amplitude near the resonant frequency point, which can be used to strengthen the suppression effect of the fixed-period detent force [25]. The quasi-PR controller transfer function can be expressed as [26]

$$G_{\mathrm{PR}}(s) = K_{\mathrm{p}} + \frac{2K_{\mathrm{R}}\omega_{\mathrm{c}}s}{s^2 + 2\omega_{\mathrm{c}}s + {\omega_0}^2} \tag{10}$$

where K_{P} is the proportional coefficient, K_{R} is the resonant coefficient, ω_{c} is the resonant bandwidth, and ω_0 is the resonant angular frequency.

According to the internal model principle, the improved ESO considering the detent force model is designed, which is called IMESO. It can not only compensate and suppress the detent force but also estimate and compensate for the other unmodeled thrust ripples in real time.

When various thrust disturbances of PMLSM are considered, its equation of motion can be expressed as

$$\begin{aligned}\dot{v} &= \frac{3\pi p_{\mathrm{n}}\psi_{\mathrm{f}}}{2\tau M}i_{\mathrm{q}} - \frac{B_{\mathrm{n}}}{M}v - \frac{F_{\mathrm{L}}}{M} + \frac{F_{\mathrm{det}}}{M} \\ &= b_0 {i_{\mathrm{q}}}^* - \frac{B_{\mathrm{n}}}{M}v - \frac{F_{\mathrm{L}}}{M} + \frac{F_{\mathrm{det}}}{M} + \left(\frac{3\pi p_{\mathrm{n}}\psi_{\mathrm{f}}}{2\tau M} - b_0\right){i_{\mathrm{q}}}^* \\ &\quad + \frac{3\pi p_{\mathrm{n}}\psi_{\mathrm{f}}}{2\tau M}(i_{\mathrm{q}} - {i_{\mathrm{q}}}^*) \\ &= b_0 {i_{\mathrm{q}}}^* + c(t) + p(t)\end{aligned} \tag{11}$$

with

$$\begin{cases} c(t) = \frac{3\pi p_{\mathrm{n}}\psi_{\mathrm{f}}}{2\tau M}i_{\mathrm{q}} - b_0 {i_{\mathrm{q}}}^* - \frac{B_{\mathrm{n}}}{M}v - \frac{F_{\mathrm{L}}}{M} \\ p(t) = \frac{F_{\mathrm{det}}}{M} \end{cases} \tag{12}$$

where b_0 is the control gain. F_{det} is the detent force. $c(t)$ is the lumped unmodeled disturbance including the load disturbance, the friction disturbance, the parameter perturbation, and the force ripple. $p(t)$ is the detent force disturbance, which can be expressed as $a\sin[(2\pi/\tau)x + \varphi] = a\sin(4\pi f t + \varphi)$, where f is the known running frequency of PMLSM, a is the unknown amplitude, and φ is the unknown phase.

Define each state variable as follows:

$$x_1 = v, x_2 = c(t), x_3 = p(t), x_4 = \frac{dp(t)}{dt}.$$

The designed internal model ESO is as follows:

$$\begin{cases} \dot{\hat{x}}_1 = \hat{x}_2 + \hat{x}_3 + b_0 i_{\mathrm{q}}^* + h_1(y - \hat{y}) \\ \dot{\hat{x}}_2 = h_2(y - \hat{y}) \\ \dot{\hat{x}}_3 = \hat{x}_4 + h_3(y - \hat{y}) \\ \dot{\hat{x}}_4 = -16\pi^2 f^2 \hat{x}_3 + h_4(y - \hat{y}) \\ \hat{y} = \hat{x}_1 \end{cases} \tag{13}$$

where $\hat{x}_1$, $\hat{x}_2$, $\hat{x}_3$, and $\hat{x}_4$ are estimate values of state variable v, $c(t)$, $p(t)$, and $dp(t)/dt$. h_1, h_2, h_3, and h_4 are four gains of IMESO.

According to (11), the control gain b_0 of the observer can be expressed as

$$b_0 = \frac{3\pi p_{\mathrm{n}} \psi_{\mathrm{f}}}{2\tau M}. \tag{14}$$

According to the thrust (1) of PMLSM at the *d*-*q* axis, the flux linkage of the permanent magnet ψ_{f} can be obtained as follows:

$$\psi_{\mathrm{f}} = \frac{2\tau F_{\mathrm{e}}}{3\pi p_{\mathrm{n}} i_{\mathrm{q}}}. \tag{15}$$

By substituting (15) into (14), the control gain b_0 can be obtained according to the thrust constant $F_{\mathrm{e}}/i_{\mathrm{q}}$ of PMLSM.

In this article, IMESO is adjusted as a fourth-order system with all the poles coincident. Then, the four parameters are adjusted by the bandwidth of the observer. The characteristic polynomial form of the target system is as follows:

$$(s + \omega)^4 = s^4 + 4\omega s^3 + 6\omega^2 s^2 + 4\omega^3 s + \omega^4. \tag{16}$$

According to (13), the characteristic polynomial $c(s)$ of IMESO can be obtained as follows:

$$\begin{aligned} c(s) = {} & s^4 + h_1 s^3 + \left(h_2 + h_3 + 16\pi^2 f^2\right) s^2 \\ & + \left(h_4 + 16\pi^2 f^2 h_1\right) s + 16\pi^2 f^2 h_2. \end{aligned} \tag{17}$$

By corresponding the coefficients of (16) and (17), the four parameter expressions of the observer can be obtained as follows:

$$\begin{cases} h_1 = 4\omega_{\mathrm{eso}} \\ h_2 = \frac{\omega_{\mathrm{eso}}^4}{16\pi^2 f^2} \\ h_3 = 6\omega_{\mathrm{eso}}^2 - 16\pi^2 f^2 - \frac{\omega_{\mathrm{eso}}^4}{16\pi^2 f^2} \\ h_4 = 4\omega_{\mathrm{eso}}^3 - 48\pi^2 f^2 \omega_{\mathrm{eso}} \end{cases} \tag{18}$$

where ω_{eso} is the bandwidth of the IMESO.

B. Convergence Analysis

The convergence of PILC is analyzed as follows. As can be seen from (9), the relationship between the *k*th and (*k*-1)th iteration learning tracking errors of PILC can be expressed as

$$\begin{aligned} \Delta v_k &= V_{\mathrm{ref}} - M(t)\left[\alpha u_{k-1}(t) + K_{\mathrm{PL1}} \Delta v_{k-1}(t) + K_{\mathrm{PL2}} \Delta v_k(t)\right] \\ &= \frac{\alpha - K_{\mathrm{PL1}} M(t)}{1 + K_{\mathrm{PL2}} M(t)} \Delta v_{k-1}(t) + \frac{(1-\alpha) v_{\mathrm{ref}}}{1 + K_{\mathrm{PL2}} M(t)} \\ &= H(t) \Delta v_{k-1}(t) + P(t). \end{aligned} \tag{19}$$

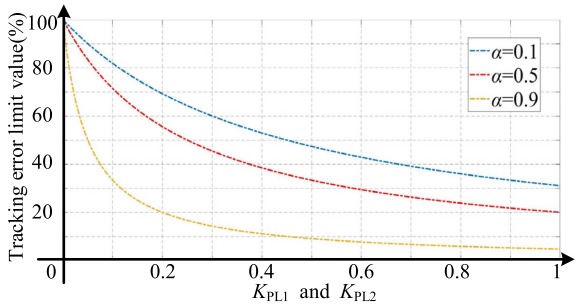

Fig. 5. Relationship of tracking error limit value to α, K_{PL1}, and K_{PL2}.

According to (19), the sufficient condition for PILC convergence is

$$|H(t)| = \left|\frac{\alpha - K_{\mathrm{PL1}} M(t)}{1 + K_{\mathrm{PL2}} M(t)}\right| < 1. \tag{20}$$

The infinite norm on both sides of (19) can be further expressed as

$$\begin{aligned} \|\Delta v_k\|_\infty &= \|H(t)\Delta v_{k-1}(t) + P(t)\|_\infty \\ &\le \|H(t)\Delta v_{k-1}(t)\|_\infty + \|P(t)\|_\infty \\ &= |H(t)|\,\|\Delta v_{k-1}(t)\|_\infty + |P(t)|_{\max} \\ &\le |H(t)|^2 \|\Delta v_{k-2}(t)\|_\infty + (1 + |H(t)|)\,|P(t)|_{\max} \le \cdots\cdots \\ &\le |H(t)|^k \|\Delta v_0(t)\|_\infty + \left(1 + \cdots\cdots + |H(t)|^{k-1}\right)|P(t)|_{\max} \\ &= |H(t)|^k \|\Delta v_0(t)\|_\infty + \frac{1 - |H(t)|^k}{1 - |H(t)|}|P(t)|_{\max}. \end{aligned} \tag{21}$$

According to (21), when the number of iterations k tends to infinity, the following expression can be obtained:

$$\begin{aligned} \lim_{k\to\infty} \|\Delta v_k\|_\infty &= \lim_{k\to\infty} \Bigg(|H(t)|^k \|\Delta v_0(t)\|_\infty \\ &\quad + \frac{1 - |H(t)|^k}{1 - |H(t)|}|P(t)|_{\max} \Bigg) \\ &= \frac{|P(t)|_{\max}}{1 - |H(t)|}. \end{aligned} \tag{22}$$

It can be seen from (22) that the tracking error of PILC has a limit value that meets the convergence condition, and its limit value is related to α, K_{PL1}, and K_{PL2}, which is shown in Fig. 5.

C. Stability and Parameter Sensitivity for PR-IMESO

The PR-IMESO consists of resonant term $R(s)$ and IMESO. Combined with (13), the total disturbance compensation can be expressed as

$$\hat{d}(t) = \hat{x}_3 + \hat{x}_2 + h_1(y - \hat{y}) + R(s)(y - \hat{y}). \tag{23}$$

According to (13) and (23), the speed estimate value and disturbance compensation value after the Laplace transform of

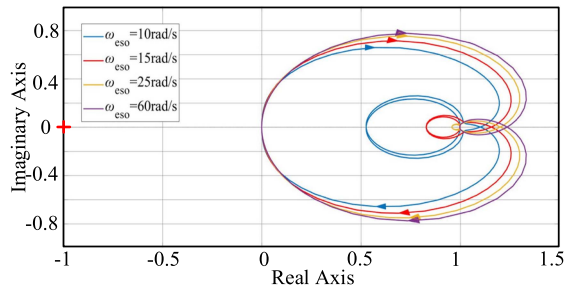

Fig. 6. Nyquist diagram of PR-IMESO when $f = 1$ Hz.

PR-IMESO can be obtained as

$$\begin{cases} s\hat{v} = b_0 i_{\mathrm{q}}^* + \hat{d}(s) \\ s\hat{d}(s) = h_2 e(s) + h_1 s e(s) + \frac{h_4 s e(s) + h_3 s^2 e(s)}{s^2 + 16\pi^2 f^2} + R(s)e(s) \end{cases}. \tag{24}$$

According to (24), the error of the system can be expressed as

$$e(s) = v(s) - \hat{v}(s) = v(s) - \frac{1}{s}\left(b_0 i_{\mathrm{q}}^*(s) + \hat{d}(s)\right). \tag{25}$$

The "total disturbance" of the system can be expressed as

$$F(s) = sv(s) - b_0 i_{\mathrm{q}}^*(s). \tag{26}$$

Where the transfer function between the compensation of PR-IMESO and the "total disturbance" of the system is investigated. Taking the observer input $i_{\mathrm{q}} = 0$, the transfer function of PR-IMESO can be obtained, as shown in (27) shown at the bottom of this page.

Since the transfer function of the observer is related to the speed, the Nyquist diagram of the observer under different running frequencies of the linear motor can be obtained according to (27).

The running frequency f is set as 1 Hz, and the bandwidth of PR-IMESO ω_{eso} is set to 10 rad/s, 15 rad/s, 25 rad/s, and 60 rad/s, respectively. Nyquist diagram of PR-IMESO is shown in Fig. 6. When the bandwidth of PR-IMESO ω_{eso} changes, the Nyquist curve of the observer never surrounds the point (-1, j0). According to the Nyquist stability criterion, it can be concluded that the studied PR-IMESO is stable.

According to the PR-IMESO transfer function in (27), the Bode diagram under different bandwidths can be obtained, as shown in Fig. 7. Obviously, with the increase of ω_{eso}, the bandwidth of the disturbance estimation increases, the gain of the observer is more stable, and the performance of the disturbance estimation is better. Since the poles of the observer transfer function are related to the observer bandwidth and the speed

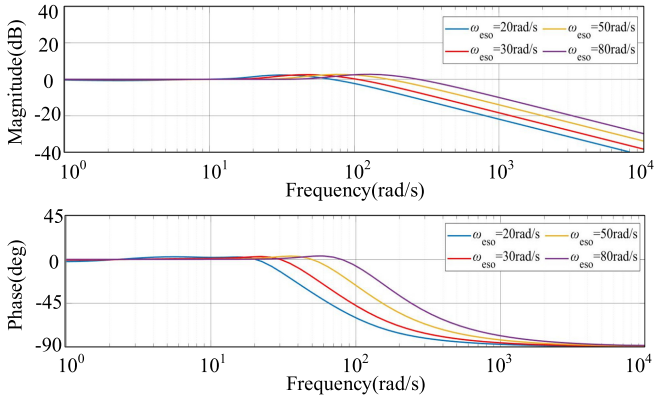

Fig. 7. Bode diagram of PR-IMESO when $f = 1$ Hz.

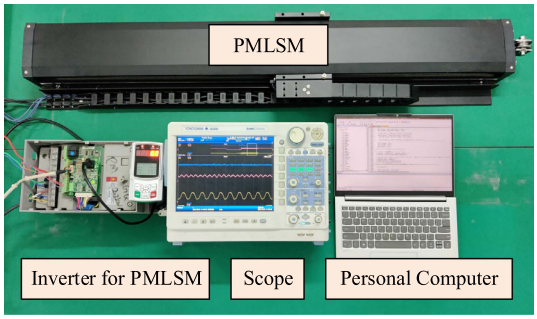

Fig. 8. Experimental platform of a 750-W PMLSM.

of PMLSM, it is necessary to determine the best bandwidth of PR-IMESO according to the actual situation of the system.

IV. Experimental Verification

To verify the feasibility and effectiveness of the proposed suppression strategy, experiments under different conditions were carried out on a 750-W PMLSM experimental platform, as shown in Fig. 8 . The main control chip uses STM32F103, the PWM switching frequency of the inverter is set to 6 kHz, and the specific parameters of test PMLSM are shown in Table I. The load is applied by weights and a pulley fixed to one side of the motor guide rail. The mover drags the weight through the steel wire rope and pulley, thus achieving the motor loading. The thrust ripple suppression strategies of PMLSM under different loads and speeds were tested on the experimental platform. Since the thrust of the mover cannot be measured directly in the experiment, the effect of thrust ripple suppression is evaluated by measuring the speed error of the mover [14], [18], [27]. The

$$G(s) = \frac{\hat{d}(s)}{F(s)} = \frac{(h_1 s + h_2)\left(s^2 + 16\pi^2 f^2\right)\left(s^2 + 2\omega_{\mathrm{c}} s + \omega_0^2\right) + \left(h_4 s + h_3 s^2\right)\left(s^2 + 2\omega_{\mathrm{c}} s + \omega_0^2\right) + 2K_{\mathrm{R}}\omega_{\mathrm{c}} s^2\left(s^2 + 16\pi^2 f^2\right)}{\left(s^2 + h_1 s + h_2\right)\left(s^2 + 16\pi^2 f^2\right)\left(s^2 + 2\omega_{\mathrm{c}} s + \omega_0^2\right) + \left(h_4 s + h_3 s^2\right)\left(s^2 + 2\omega_{\mathrm{c}} s + \omega_0^2\right) + 2K_{\mathrm{R}}\omega_{\mathrm{c}} s^2\left(s^2 + 16\pi^2 f^2\right)}. \tag{27}$$

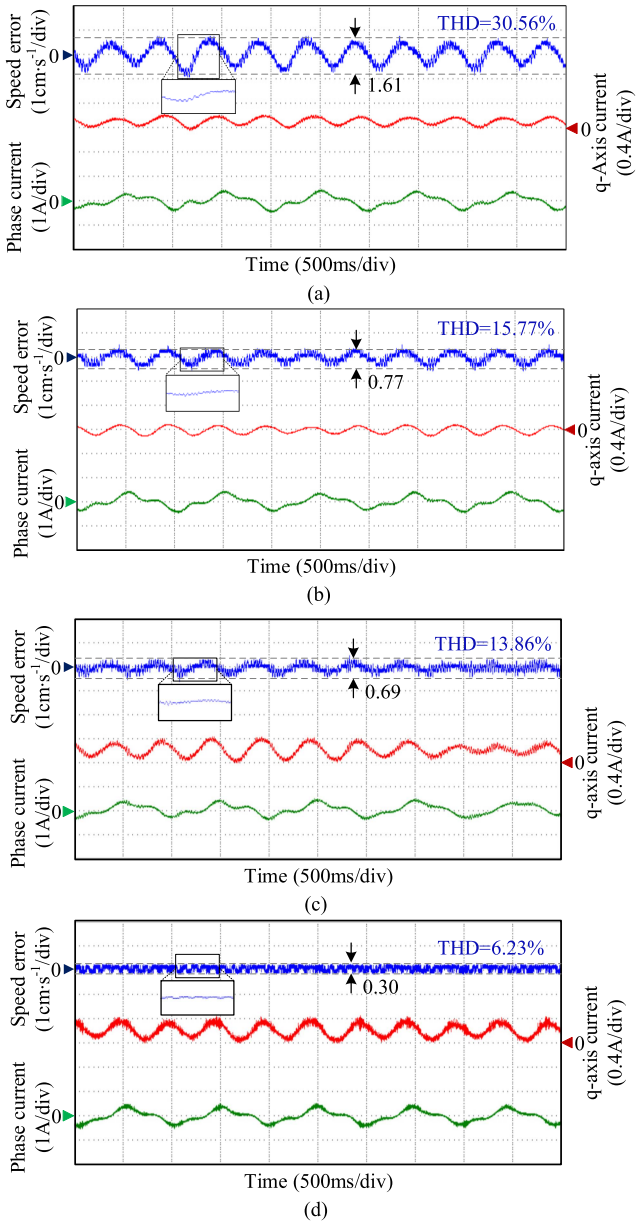

Fig. 9. Experimental results at 3 cm/s under no-load conditions. (a) With no suppression strategy. (b) With PILC. (c) With PILC+LESO. (d) With PILC+PR-IMESO.

parameters of the iterative learning controller are set to $\alpha = 0.97$, $K_{\mathrm{PL1}} = 1.3$, and $K_{\mathrm{PL2}} = 1.3$, and the parameters of PR-IMESO are set to $\omega_{\mathrm{eso}} = 15$, $K_{\mathrm{R}} = 100$, and $\omega_{\mathrm{c}} = 0.628$ rad/s.

First, the proposed suppression strategy is verified under no-load conditions. Fig. 9 shows experimental results at 3 cm/s under no-load conditions. As can be seen from Fig. 9(a), without any suppression strategy, there is a large complex fluctuation in the speed error of the mover, whose fluctuation amplitude is 1.61 cm/s, and the frequency of the main component is twice the frequency of the phase current. In Fig. 9(b), when PILC is adopted, the amplitude of the speed fluctuation decreases to 0.77 cm/s and the suppression rate is 52.2%. The amplitude of the speed fluctuation decreases obviously, but it still contains the second-order component with a large amplitude. So, it cannot

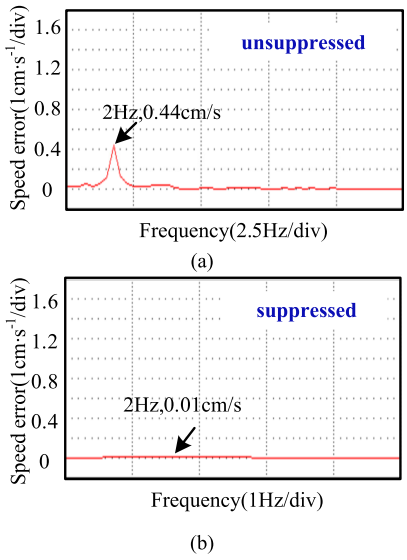

Fig. 10. FFT analysis results of unsuppressed and suppressed speed errors under no-load conditions. (a) With no suppression strategy. (b) With PILC+PR-IMESO.

TABLE I
PMLSM PARAMETERS

Parameters	Value
Continuous current (A_{rms})	2.1
Thrust constant (N/A_{rms})	48.6
line resistance (Ω)	8.4
Interwire inductance (mH)	37.1
Pole pitch (mm)	15
Mover mass (kg)	0.7

achieve the ideal suppression effect. For comparison, experiment results of the LESO-based ILC method are also presented. As can be seen from Fig. 9(c), when LESO-based PILC is adopted, the amplitude of the speed fluctuation is reduced to 0.69 cm/s and the suppression rate is 57.1%. Differently, in Fig. 9(d), when the PR-IMESO-based PILC suppression strategy is adopted, the speed fluctuation of the mover is greatly reduced, the fluctuation amplitude is reduced to 0.3 cm/s, and the suppression rate reaches 81.4%.

To prove that the second-order thrust ripple is suppressed, the fast Fourier transform (FFT) analysis results of unsuppressed and suppressed speed errors under on-load conditions are given in Fig. 10. As can be seen from Fig. 10(a), the dominant harmonic component of the unsuppressed speed error is the second harmonic, whose amplitude value is 0.44 cm/s. But in Fig. 10(b), with the proposed method, the amplitude value of the second harmonic is reduced to 0.01 cm/s. The suppression rate of the second-order thrust ripple is 97.7%.

The effectiveness of the proposed suppression strategy under load conditions is further verified. Fig. 11 shows experimental results at 3 cm/s under 30-N load conditions. As can be seen from Fig. 11(a), without any suppression strategy, the amplitude of the mover speed fluctuation is 1.62 cm/s. In Fig. 11(b), when PILC is adopted, the amplitude of the speed fluctuation is reduced to 0.84 cm/s, and the suppression rate is 48.1%. As can be seen from Fig. 11(c), when LESO-based ILC is adopted, the amplitude of

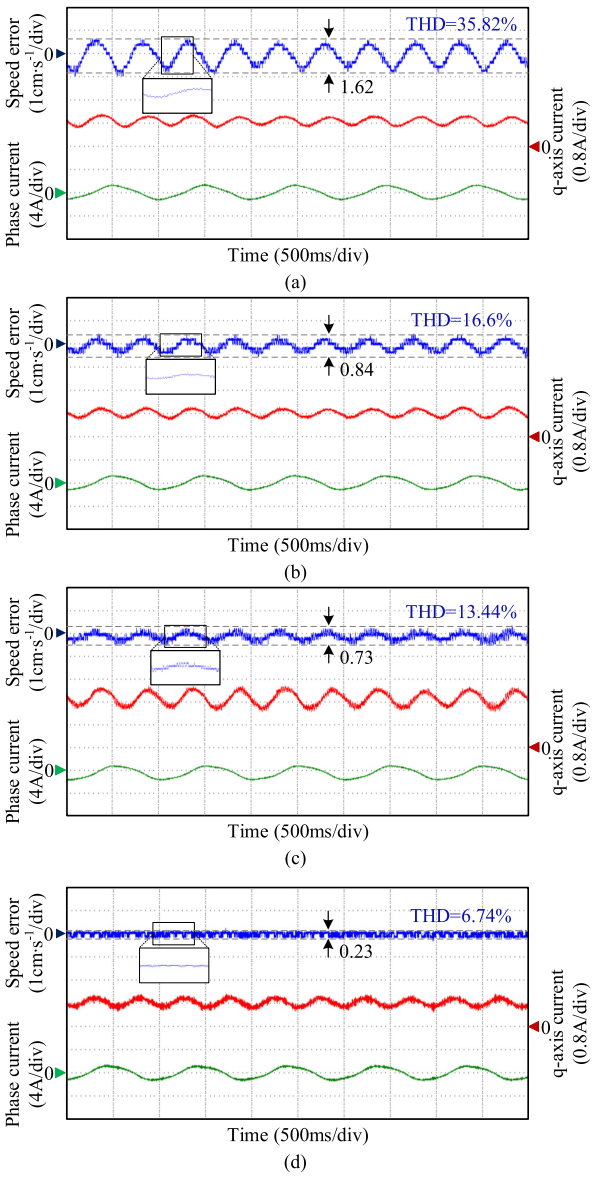

Fig. 11. Experimental results at 3 cm/s under 30-N load condition. (a) With no suppression strategy. (b) With PILC. (c) With PILC+LESO. (d) With PILC+PR-IMESO.

the speed fluctuation is reduced to 0.73 cm/s and the suppression rate is 54.9%. But in Fig. 11(d), after the PR-IMESO-based PILC suppression strategy is added, the mover speed fluctuation is greatly reduced and the speed error waveform is almost flat. The fluctuation amplitude is reduced to 0.23 cm/s and the suppression rate reaches 85.8%. The experimental results show that compared with the LESO-based ILC method, the proposed method obviously has a better suppression effect. PR-IMESO-based PILC thrust ripple suppression strategy has a satisfactory mover thrust ripple suppression effect under no-load and load conditions, which verifies its rationality and effectiveness.

Fig. 12 shows the FFT analysis results of unsuppressed and suppressed speed errors under 30-N load conditions. As can be seen from Fig. 12(a), the amplitude value of the second harmonic is 0.49 cm/s. But in Fig. 12(b), with the proposed method, the

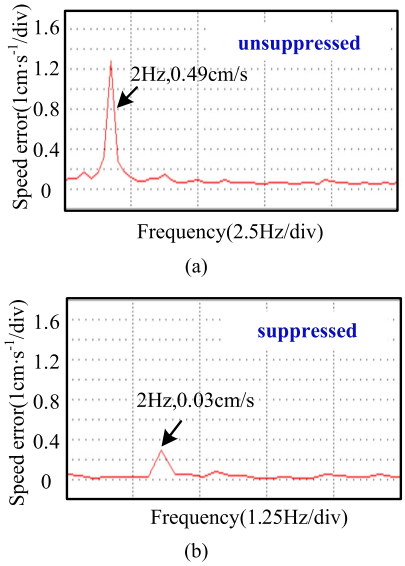

Fig. 12. FFT analysis results of unsuppressed and suppressed speed errors under 30N-load condition. (a) With no suppression strategy. (b) With PILC+PR-IMESO.

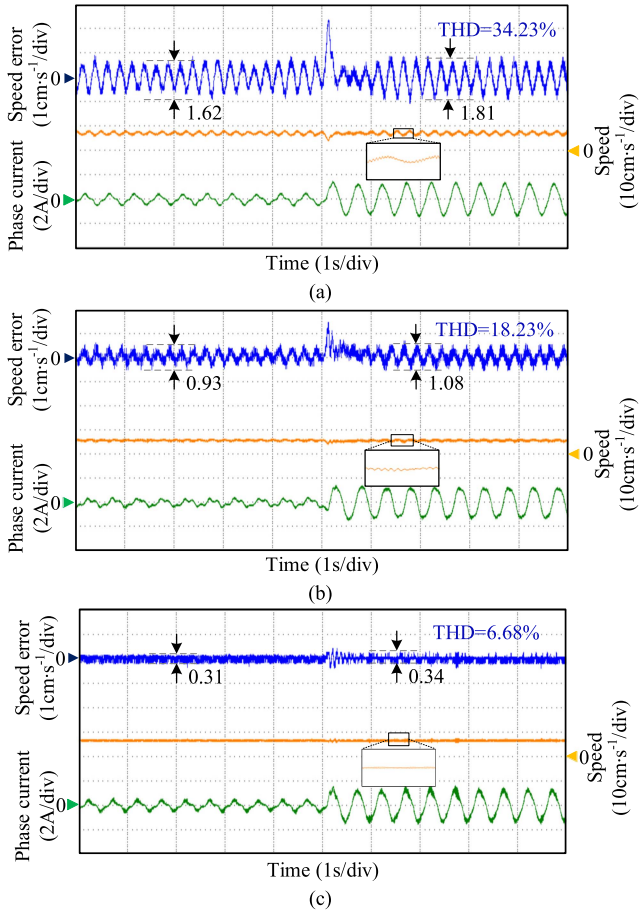

Fig. 13. Experimental results at 6 cm/s under the sudden 30-N load. (a) With no suppression strategy. (b) With PILC. (c) With PILC+PR-IMESO.

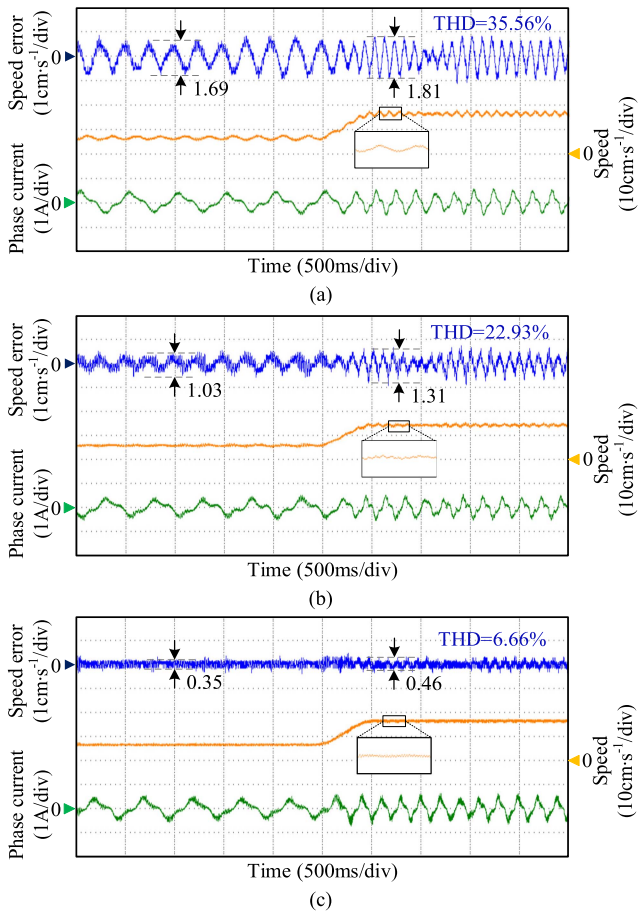

Fig. 14. Experimental results when the given speed changes from 6 to 15 cm/s under no-load conditions. (a) With no suppression strategy. (b) With PILC. (c) With PILC+PR-IMESO.

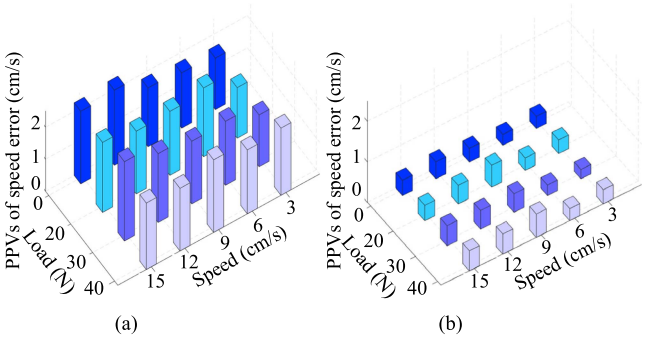

Fig. 15. Summary of experimental results under different load and speed conditions. (a) With no suppression strategy. (b) With PILC+PR-IMESO.

amplitude value of the second harmonic is reduced to 0.03 cm/s. Accordingly, the suppression rate of the detent force reaches 93.9%.

Fig. 13 shows an experimental comparison with the sudden 30-N load at 6 cm/s. In Fig. 13(a), without the proposed strategy, the mover speed error before and after the sudden load both has a large fluctuation, and the mover speed has a great drop at the sudden load time. In Fig. 13(b), with the PILC strategy, the fluctuation of the mover speed is reduced but still noticeable. The mover speed also has a drop at the sudden load time. As can be seen from Fig. 13(c), when the proposed suppression strategy is adopted, the fluctuation of the mover speed before and after the sudden load is greatly reduced, and the suppression effect is significant. In addition, the dropping of the mover speed is obviously reduced at sudden load time, and the transient process is smooth, with good dynamic performance.

Fig. 14 shows experimental results when the given speed changes from 6 to 15 cm/s. As can be seen from Fig. 14(a), when no suppression strategy is added, there is a large and complex fluctuation of the mover speed before and after the given speed mutation. In Fig. 14(b), with the PILC strategy, the fluctuation of the mover speed is also noticeable before and after the given speed mutation. However, in Fig. 14(c), with the proposed suppression strategy, the mover speed fluctuation before and after the given speed mutation is greatly reduced, and the transition of the mover speed error is smooth and rapid during the given speed mutation.

To verify whether the proposed suppression strategy in this article can play an effective role in suppression thrust ripples of the mover, experiments were carried out under different working conditions. The experimental results are summarized as shown in Fig. 15. As can be seen from Fig. 15(a), without suppression strategy, the mover speed fluctuates greatly under different speed and load conditions, and the maximum fluctuation amplitude reaches 2.4 cm/s. But in Fig. 15(b), when the proposed suppression strategy is adopted, the fluctuation of the mover speed under all working conditions is effectively suppressed, with the minimum fluctuation amplitude falling to 0.23 cm/s, the highest suppression rate reaching 87%, and the average suppression rate reaching 80.5%. Therefore, the proposed PR-IMESO-based PILC thrust ripple suppression strategy has a great suppression effect under different speed and load conditions, and its feasibility and effectiveness have been verified.

V. Conclusion

To solve the thrust ripple problem of PMLSM, this article proposed a PR-IMESO-based PILC suppression strategy. First, a P-type ILC with the forgetting factor was constructed to suppress the detent force, which is the main component of thrust ripples, and periodic force ripples. On this basis, PR-IMESO considering the detent force model was studied and designed to further suppress the detent force and residual unmodeled thrust ripples. In addition, the convergence, stability, and parameter sensitivity of the suppression strategy were analyzed at length. Although the proposed method includes iterative learning and resonant controllers, it does not increase much calculation load to the chip. The proposed strategy has a satisfactory overall suppression effect on the thrust ripples of PMLSM. The experimental results were consistent with the theoretical analysis, which verified the rationality and effectiveness of the proposed suppression strategy. The average suppression rate of the mover speed fluctuation can reach 80.5%.

REFERENCES

[1] M. Wang, L. Li, D. Pan, Y. Tang, and Q. Guo, "High-bandwidth and strong robust current regulation for PMLSM drives considering thrust ripple," *IEEE Trans. Power Electron.*, vol. 31, no. 9, pp. 6646–6657, Sep. 2016.

[2] M. Wang, K. Kang, C. Zhang, and L. Li, "Precise position control in air-bearing PMLSM system using an improved anticipatory fractional-order iterative learning control," *IEEE Trans. Ind. Electron.*, vol. 71, no. 6, pp. 6073–6083, Jun. 2024.

[3] X. Fang, L. Wang, and K. Zhang, "High order nonsingular fast terminal sliding mode control of permanent magnet linear motor based on disturbance observer," *Trans. China Electrotech. Soc.*, vol. 38, no. 2, pp. 409–421, Jan. 2023.

[4] R. Yang, M. Wang, L. Li, Y. Zenggu, and J. Jiang, "Integrated uncertainty/disturbance compensation with second-order sliding-mode observer for PMLSM-driven motion stage," *IEEE Trans. Power Electron.*, vol. 34, no. 3, pp. 2597–2607, Mar. 2019.

[5] H. Wang, Z. Zhang, and C. Liu, "Detent force analysis and experiment for permanent magnet linear synchronous motor," *Proc. CSEE*, vol. 30, no. 15, pp. 58–63, May 2010.

[6] X. Z. Huang, J. Li, C. Zhang, Z. Y. Qian, L. Li, and D. Gerada, "Electromagnetic and thrust characteristics of double-sided permanent magnet linear synchronous motor adopting staggering primaries structure," *IEEE Trans. Ind. Electron.*, vol. 66, no. 6, pp. 4826–4836, Jun. 2019.

[7] C. Zhang, L. Zhang, X. Huang, J. Yang, and L. Shen, "Research on the method of suppressing the end detent force of permanent magnet linear synchronous motor based on stepped double auxiliary pole," *IEEE Access*, vol. 8, pp. 112539–112552, 2020.

[8] L. Bascetta, P. Rocco, and G. Magnani, "Force ripple compensation in linear motors based on closed-loop position-dependent identification," *IEEE/ASME Trans. Mechatron.*, vol. 15, no. 3, pp. 349–359, Jun. 2010.

[9] H.-S. Ahn, Y. Chen, and H. Dou, "State-periodic adaptive compensation of cogging and coulomb friction in permanent-magnet linear motors," *IEEE Trans. Magn.*, vol. 41, no. 1, pp. 90–98, Jan. 2005.

[10] T.-S. Hwang and J.-K. Seok, "Observer-based ripple force compensation for linear hybrid stepping motor drives," *IEEE Trans. Ind. Electron.*, vol. 54, no. 5, pp. 2417–2424, Oct. 2007.

[11] Z. He et al., "Thrust ripple reduction in permanent magnet synchronous linear motor based on tuned viscoelastic damper," *IEEE Trans. Ind. Electron.*, vol. 66, no. 2, pp. 977–987, Feb. 2019.

[12] C. Zhang et al., "A low detent force DS-PMSLM based on the modulation of cogging and end forces," *IEEE Trans. Ind. Electron.*, vol. 70, no. 1, pp. 721–730, Jan. 2023.

[13] Y.-W. Zhu and Y.-H. Cho, "Thrust ripples suppression of permanent magnet linear synchronous motor," *IEEE Trans. Magn.*, vol. 43, no. 6, pp. 2537–2539, Jun. 2007.

[14] Y.-W. Zhu, S.-M. Jin, K.-S. Chung, and Y.-H. Cho, "Control-based reduction of detent force for permanent magnet linear synchronous motor," *IEEE Trans. Magn.*, vol. 45, no. 6, pp. 2827–2830, Jun. 2009.

[15] F. Song, Y. Liu, J.-X. Xu, X. Yang, P. He, and Z. Yang, "Iterative learning identification and compensation of space-periodic disturbance in PMLSM systems with time delay," *IEEE Trans. Ind. Electron.*, vol. 65, no. 9, pp. 7579–7589, Sep. 2018.

[16] G. Meng, H. Yu, M. Hu, H. Liu, and C. Jiu, "Thrust ripple suppression for linear flux-switching permanent magnet machine based on a repetitive control strategy of nonlinear feedback," *Trans. China Electrotech. Soc.*, vol. 32, no. 8, pp. 169–177, Apr. 2017.

[17] G. Bi, G. Zhang, G. Wang, Q. Wang, Y. Hu, and D. Xu, "Adaptive iterative learning control-based rotor position harmonic error suppression method for sensorless PMSM drives," *IEEE Trans. Ind. Electron.*, vol. 69, no. 11, pp. 10870–10881, Nov. 2022.

[18] K. Cho, J. Kim, S. B. Choi, and S. Oh, "A high-precision motion control based on a periodic adaptive disturbance observer in a PMLSM," *IEEE/ASME Trans. Mechatron.*, vol. 20, no. 5, pp. 2158–2171, Oct. 2015.

[19] R. Yang, L. Li, M. Wang, and C. Zhang, "Force ripple compensation and robust predictive current control of PMLSM using augmented generalized proportional–integral observer," *IEEE J. Emerg. Sel. Topics Power Electron.*, vol. 9, no. 1, pp. 302–315, Feb. 2021.

[20] X. Liu, H. Cao, W. Wei, J. Wu, B. Li, and Y. Huang, "A practical precision control method base on linear extended state observer and friction feedforward of permanent magnet linear synchronous motor," *IEEE Access*, vol. 8, pp. 68226–68238, 2020.

[21] C. Liu, G. Luo, Z. Xue, Z. Zhou, and Z. Chen, "A PMSM speed servo system based on internal model control with extended state observer," in *Proc. IEEE 43rd Annu. Conf. Ind. Electron.*, 2017, pp. 1729–1734.

[22] H. Hu, X. Liu, J. Zhao, and Y. Guo, "Analysis and minimization of detent end force in linear permanent magnet synchronous machines," *IEEE Trans. Ind. Electron.*, vol. 65, no. 3, pp. 2475–2486, Mar. 2018.

[23] C. Zhang, L. Zhang, X. Huang, J. Yang, and L. Shen, "Research on the method of suppressing the end detent force of permanent magnet linear synchronous motor based on stepped double auxiliary pole," *IEEE Access*, vol. 8, pp. 112539–112552, 2020.

[24] X. Z. Huang et al., "Detent-force minimization of double-sided permanent magnet linear synchronous motor by shifting one of the primary components," *IEEE Trans. Ind. Electron.*, vol. 67, no. 1, pp. 180–191, Jan. 2020.

[25] W.-K. Sou, C.-W. Chao, C. Gong, C.-S. Lam, and C.-K. Wong, "Analysis, design, and implementation of multi-quasi-proportional-resonant controller for thyristor-controlled LC-coupling hybrid active power filter (TCLC-HAPF)," *IEEE Trans. Ind. Electron.*, vol. 69, no. 1, pp. 29–40, Jan. 2022.

[26] Q. An, J. Zhang, Q. An, and A. Shamekov, "Quasi-proportional-resonant controller based adaptive position observer for sensorless control of PMSM drives under low carrier ratio," *IEEE Trans. Ind. Electron.*, vol. 67, no. 4, pp. 2564–2573, Apr. 2020.

[27] Z. Q. Zhu, S. Ruangsinchaiwanich, Y. Chen, and D. Howe, "Evaluation of superposition technique for calculating cogging torque in permanent-magnet brushless machines," *IEEE Tran. Magn.*, vol. 42, no. 5, pp. 1597–1603, May 2006.

Guoqiang Zhang (Senior Member, IEEE) received the B.S. degree in electrical engineering from Harbin Engineering University, Harbin, China, in 2011, and the M.S. and Ph.D. degrees in electrical engineering from Harbin Institute of Technology, Harbin, China, in 2013 and 2017, respectively.

Since 2017, he has been with the Department of Electrical Engineering, Harbin Institute of Technology, where he is currently a Professor. His research interests include control of electrical drives and parameter identification techniques, with a main focus on sensorless field-oriented control of synchronous motor drives.

Dr. Zhang is an Associate Editor for the *Journal of Power Electronics*.

Xinru Zhao received the B.S. degree in electrical engineering in 2022 from the Harbin Institute of Technology (HIT), Harbin, China, where she is currently working toward the M.S. degree in electrical engineering with the School of Electrical Engineering and Automation.

Her current research interests include the control of permanent magnet synchronous linear motor drives.

Qiwei Wang(Member, IEEE) received the B.S., M.S., and Ph.D. degrees in electrical engineering from the Harbin Institute of Technology, Harbin, China, in 2015, 2017, and 2022, respectively.

He is currently a postdoctoral researcher in power electronics and electrical drives with the School of Electrical Engineering and Automation, Harbin Institute of Technology. His research interests include parameter identification techniques and PMSM position sensorless control.

Dawei Ding (Member, IEEE) received the B.S. and M.S. degrees in electrical engineering from Hefei University of Technology, Hefei, China, in 2014 and 2017, respectively, and the Ph.D. degree in electrical engineering from Harbin Institute of Technology (HIT), Harbin, China, in 2021.

From 2020 to 2021, he was a visiting Ph.D. student with the Technical University of Denmark. He is currently an Associate Professor with the School of Electrical Engineering and Automation, HIT. He authored more than 30 journal papers in IEEE transactions and held several authorized Chinese invention patents. His research interests include advanced control of permanent magnet synchronous motor drives and electrolytic capacitorless ac motor drives.

Binxing Li (Member, IEEE) received the B.S. and Ph.D. degrees in electrical engineering from the Harbin Institute of Technology (HIT), Weihai, China, in 2017 and 2022, respectively.

He is currently a postdoctoral researcher with the School of Electrical Engineering and Automation, HIT. His research interests include permanent magnet synchronous motor drives, high-efficiency ac–dc converters, and the application of GaN power devices.

Gaolin Wang (Senior Member, IEEE) received the B.S., M.S., and Ph.D. degrees in electrical engineering from the Harbin Institute of Technology, Harbin, China, in 2002, 2004, and 2008, respectively.

In 2009, he joined the Department of Electrical Engineering, Harbin Institute of Technology, as a Lecturer, where he has been a Full Professor of Electrical Engineering since 2014. From 2009 to 2012, he was a Postdoctoral Fellow with Shanghai Step Electric Corporation, where he was involved in the traction machine control for direct-drive elevators. He authored more than 60 technical papers published in IEEE transactions. He is the holder of 30 Chinese patents. His research interests include permanent magnet synchronous motor drives, position sensorless control of ac motors, and digital control of power converters.

Dr. Wang is a Guest Associate Editor of IEEE TRANSACTIONS ON INDUSTRIAL ELECTRONICS, and an Associate Editor of IEEE TRANSACTIONS ON TRANSPORTATION ELECTRIFICATION, *IET Electric Power Applications*, and *Journal of Power Electronics*.

Dianguo Xu (Fellow, IEEE) received the B.S. degree in control engineering from Harbin Engineering University, Harbin, China, in 1982, and the M.S. and Ph.D. degrees in electrical engineering from the Harbin Institute of Technology (HIT), Harbin, China, in 1984 and 1989, respectively.

In 1984, he joined the Department of Electrical Engineering, HIT, as an Assistant Professor. Since 1994, he has been a Professor with the Department of Electrical Engineering, HIT. He was the Dean of the School of Electrical Engineering and Automation, HIT, from 2000 to 2010, and the Assistant President from 2010 to 2014. He is currently the Vice President of the HIT. He authored or coauthored more than 600 technical papers. His research interests include renewable energy generation technology, power quality mitigation, sensorless vector-controlled motor drives, and high-performance PMSM servo systems.

Dr. Xu is the Chairman of the IEEE Harbin Section, the Co-EIC of IEEE TRANSACTIONS ON POWER ELECTRONICS, and an Associate Editor for the IEEE TRANSACTIONS ON INDUSTRIAL ELECTRONICS, and IEEE JOURNAL OF EMERGING AND SELECTED TOPICS IN POWER ELECTRONICS. He was the recipient of the 2018 IEEE IAS Outstanding Achievement Award.